4. J. Alvarez and D. R. Smyth, in Arabidopsis: *An Atlas of Morphology and Development*, J. L. Bowman, Ed. (Springer-Verlag, New York, 1994).
5. S. E. Clark, M. P. Running, E. M. Meyerowitz, *Development* **121**, 2057 (1995).
6. J. M. Kayes and S. E. Clark, *ibid.* **125**, 3843 (1998).
7. The *clv3-1* and *clv3-2* alleles have been described (*4*, *5*). The *clv3-3* allele was identified in line CS6421 from the Ohio State *Arabidopsis* Biological Resource Center. The *clv3-4* allele was isolated by G. Redei and donated to the Ohio State *Arabidopsis* Biological Resource Center under the designation CS3603. The *clv3-5* allele was identified in an EMS mutagenesis of *cuc2* mutant plants in the Landsberg *erecta* ecotype. The *clv3-6* allele was identified in an EMS mutagenesis of 35S::PI transgenic plants in the Nossen ecotype. Plants were grown and maintained as described (*5*).
8. S. E. Clark, R. W. Williams, E. M. Meyerowitz, *Cell* **89**, 575 (1997).
9. B. Kobe and J. Deisenhofer, *Trends Biochem. Sci.* **19**, 415 (1994); S. G. S. C. Buchanan and N. J. Gay, *Prog. Biophys. Mol. Biol.* **65**, 1 (1996).
10. K. A. Feldmann and M. D. Marks, *Mol. Gen. Genet.* **208**, 1 (1987).
11. E. Wisman, G. H. Cardon, P. Fransz, H. Saedler, *Plant Mol. Biol.* **37**, 989 (1998).
12. Genomic DNA flanking the *En-1* insertion site of *clv3-7* was amplified by Tail PCR (polymerase chain reaction) according to standard protocols and used to screen a wild-type Columbia library to identify genomic clones. In addition, a genomic library was made from *clv3-3* plant DNA by Sau 3A partial digestion and ligation into λGEM11 (Promega). The library was screened with T-DNA border sequence probes, and positive clones were hybridized to Southern blots to detect flanking genomic DNA. A single clone containing T-DNA and bordering genomic sequences was used to probe a wild-type Columbia genomic library in λGEM11. Sac I restriction fragments comprising 24 kb of flanking genomic DNA were subcloned into pBluescriptIISK$^+$ (Stratagene), and two subclones containing the *CLV3* region were double-strand sequenced. Nucleotide sequencing was performed with the ABI PRISM Ready Reaction Kit (Perkin-Elmer) and synthetic oligonucleotides on an ABI Automated Cycle Sequencer machine. The entire *CLV3* coding region, plus 800 bp of 5′ sequence and 1 kb of 3′ sequence, was sequenced at least once on each strand. 5′ rapid amplification of cDNA ends (RACE) was performed with primers CLV3B (5′-CTTGGTGGGTTCACATGATGG) and CLV3C (5′-GTGCAAGGGTCAGGTCC) with the 5′RACE System (Gibco-BRL) according to the manufacturer's protocol. 3′ RACE was performed with primer oli3.6 (5′-GGAAAGTGAATGGGTTGGAGC) according to standard protocols.
13. To identify mutations in the EMS-induced alleles, we amplified the *CLV3* coding region by PCR. PCR products were purified with the QIAquick PCR Purification Kit (Qiagen) and directly sequenced. Products from three independent PCR amplifications were sequenced from each wild-type and mutant genotype.
14. To identify lesions in the *clv3-2* and *clv3-4* alleles, we digested wild-type and mutant genomic DNA with multiple restriction enyzmes and performed Southern blot analysis.
15. G. von Heijne, *Nucleic Acids Res.* **14**, 4683 (1986).
16. K. Nakai and M. Kanehisa, *Genomics* **14**, 897 (1992).
17. R. N. Stewart, in *The Clonal Basis of Development*, S. Subtelny and I. M. Sussex, Eds. (Academic Press, New York, 1978).
18. R. A. E. Tilney-Bassett, *Plant Chimeras* (Arnold, London, 1986).
19. Supplemental Web material is available at www.sciencemag.org/feature/data/ 987103.shl.
20. For nonradioactive in situ hybridization, samples were treated as described [D. Bradley, R. Carpenter, H. Sommer, N. Hartley, E. Coen, *Cell* **72**, 85 (1993)]. For radioactive in situ hybridization, samples were treated as described [H. Sakai, L. J. Medrano, E. M. Meyerowitz, *Nature* **378**, 199 (1995)]. The full-length *CLV3* cDNA cloned in either the sense or antisense orientation relative to the T7 promoter was used as a template for probe synthesis with T7 RNA polymerase.
21. M. K. Barton and R. S. Poethig, *Development* **119**, 823 (1993).
22. D. R. Smyth, J. L. Bowman, E. M. Meyerowitz, *Plant Cell* **2**, 755 (1990).
23. J. A. Long and M. K. Barton, *Development* **125**, 3027 (1998).
24. R. W. Williams and E. M. Meyerowitz, personal communication.
25. P. Becraft, *Trends Plant. Sci.* **3**, 384 (1998).
26. We thank E. Wisman, B. Williams, and S. Jacobsen for *clv3* alleles, the *Arabidopsis* Biological Resource Center at Ohio State University for seeds, J. Wong and N. Beinert for technical assistance, B. Williams for sharing unpublished data, and members of the Meyerowitz Lab for discussion. This work was supported by the U.S. National Institutes of Health (J.C.F.), the Howard Hughes Medical Institute (M.P.R.), the Deutsche Forschungsgemeinschaft (SFB 243, R.S. and U.B.), the National Science Foundation (E.M.M.), and Zeneca Seeds (E.M.M.).

15 December 1998; accepted 24 February 1999

Crystal Structure of Human ZAG, a Fat-Depleting Factor Related to MHC Molecules

Luis M. Sánchez,[1]* Arthur J. Chirino,[1,2]* Pamela J. Bjorkman[1,2]†

Zn-α_2-glycoprotein (ZAG) is a soluble protein that is present in serum and other body fluids. ZAG stimulates lipid degradation in adipocytes and causes the extensive fat losses associated with some advanced cancers. The 2.8 angstrom crystal structure of ZAG resembles a class I major histocompatibility complex (MHC) heavy chain, but ZAG does not bind the class I light chain β_2-microglobulin. The ZAG structure includes a large groove analogous to class I MHC peptide binding grooves. Instead of a peptide, the ZAG groove contains a nonpeptidic compound that may be implicated in lipid catabolism under normal or pathological conditions.

ZAG is a soluble protein whose name derives from its tendency to precipitate with zinc salts and its electrophoretic mobility in the region of the α_2 globulins (*1*). ZAG is normally present in most body fluids including serum, sweat, saliva, cerebrospinal fluid, seminal plasma, milk, amniotic fluid, and urine (*1*). In addition, ZAG accumulates in breast cysts as well as in 40% of breast carcinomas, and is induced by glucocorticoids and androgens in breast cancer cell lines. Hence, ZAG may participate in breast diseases, including cancer (*2*).

The function of ZAG was elucidated when a lipid-catabolizing factor with the same amino acid sequence as ZAG was isolated from the urine of cancer patients with cachexia (*3*). Cachexia is a wasting syndrome caused by depletion of muscle and adipose tissue that is present in the majority of patients with cancer, AIDS, and other life-threatening diseases (*3*). ZAG appears to be responsible for the fat-depletion component of cachexia, since it stimulates lipid breakdown in adipocytes and reduces fat stores in laboratory animals (*3*). ZAG is overexpressed in carcinomas that induce fat loss but not in other tumors. Application of ZAG to adipocyte membranes activates a guanosine triphosphate–dependent adenylate cyclase activity, perhaps through direct or indirect interactions with a G protein–coupled receptor (*3*). Thus, its mode of action could be similar to that of lipolytic hormones. These results suggest that ZAG normally functions to regulate lipid degradation, which increases to a pathological extent in cachexia.

ZAG shares 30 to 40% amino acid sequence identity with the extracellular portions of class I major histocompatibility complex (MHC) heavy chains (*4*). Class I MHC molecules present peptide antigens to cytotoxic T cells (*5*). Other proteins related to class I MHC molecules include CD1, which presents hydrophobic antigens to T cells (*6*), the neonatal Fc receptor (FcRn), which transports immunoglobulin G across epithelia (*7*), and HFE, which binds transferrin receptor and regulates iron homeostasis (*8*). These MHC homologs are membrane-bound heterodimers that use the soluble protein β_2-microglobulin (β_2M) as a light chain. ZAG, however, is a secreted protein, and it does not associate with β_2M (*9*). The latter property is shared by MIC-A, a divergent membrane-bound member of the class I family (*10*).

Like FcRn (*11*), HFE (*11*), and MIC-A (*10*), ZAG does not bind endogenous peptides (*9*), but it appears to carry a small proteinase-resistant compound whose injection induces glomerulonephritis in experimental animals (*12*). In peptide-binding class I MHC molecules, a large groove located between two α helices in the α1-α2 superdomain of the heavy chain serves as the binding site (*5*). An analogous groove acts as the antigen binding site in CD1,

[1]Division of Biology 156-29 and [2]Howard Hughes Medical Institute, California Institute of Technology, Pasadena, CA 91125, USA.

*These authors contributed equally to this work.
†To whom correspondence should be addressed. E-mail: bjorkman@cco.caltech.edu

but is narrowed in HFE and closed in FcRn, the class I–related proteins that do not bind small molecular weight ligands (*11*).

Here, we present the 2.8 Å crystal structure of human ZAG, which reveals an MHC-like fold without a β_2M light chain and a groove that closely resembles the peptide-binding sites of classical class I MHC molecules. Rather than containing a peptide, the

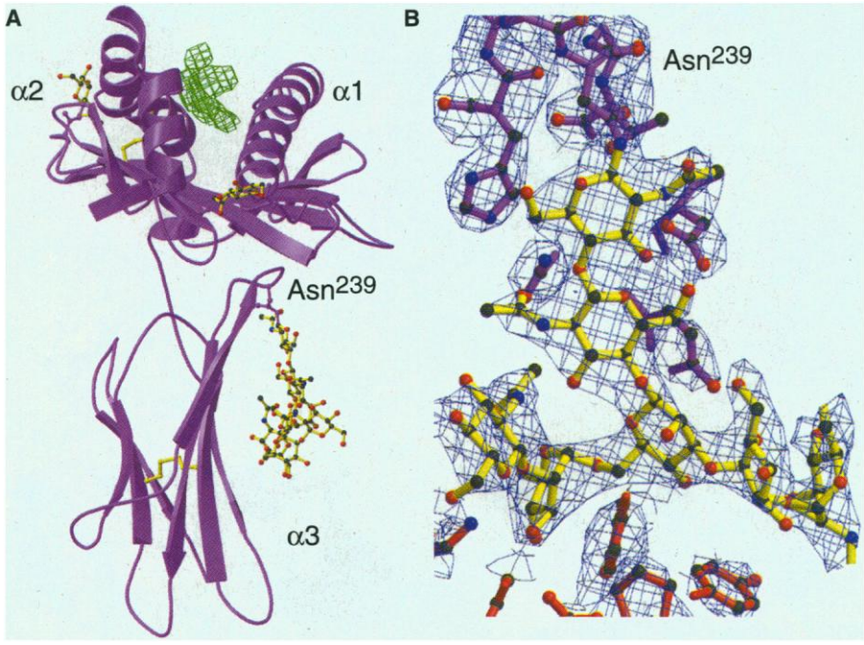

Fig. 1. (**A**) Ribbon diagram of the structure of human ZAG. Density corresponding to the nonpeptidic ligand is shown in green as derived from a 2.9 Å MIRAS, NCS averaged, figure-of-merit weighted electron density map contoured at 1σ. Ordered N-linked carbohydrates are shown in ball-and-stick representation. (**B**) The ZAG model (molecule 2) in the region of the N-linked carbohydrate attached to Asn^{239} superimposed on a 2.8 Å SIGMAA-weighted $2F_o - F_c$ annealed omit electron density map (*13*). The carbohydrate electron density at Asn^{239} shows nine carbohydrate residues arranged in a biantennary structure (*14*) (two of the carbohydrate residues are omitted from the figure for clarity). The large number of ordered carbohydrate residues at Asn^{239} is likely to result from stabilization of the flexible carbohydrate by crystal contacts with protein residues in symmetry-related ZAG molecules (shown in red sticks; bottom). Figures were made as described (*23*).

Table 1. Data collection, heavy-atom phasing, and refinement statistics for ZAG. Statistics in parentheses refer to the highest resolution bin. ZAG was crystallized in space group $P2_12_12$ with four molecules per asymmetric unit and cryoprotected as described (*9*). Native and heavy-atom derivative data sets were collected at −165°C from multiple crystals using an R-AXIS IIc imaging plate system mounted on a Rigaku R200 rotating anode generator. Data were processed and scaled with the HKL package (*13*). Heavy-atom refinement was done with SHARP (*13*), which treated different data sets of derivatives with the same sites as separate "crystals" of the same "compound" and refined separate heavy-atom occupancies and temperature factors for each "crystal" data set. Electron density maps calculated from MIRAS phases derived from all eight heavy-atom data sets were superior to maps derived from various combinations of mercury and platinum data sets. Eight NCS operators were determined from least squares superposition of HLA-A2 α1-α2 and α3 domains manually placed in the electron density, four relating the α1-α2 regions and four relating the α3 domains. After solvent flipping using Solomon (*13*), subdomain NCS averaging of the four molecules and phase extension from 5.0 to 2.9 Å were carried out with DM in the CCP4 suite (*13*) (final average correlation >0.8). When the same averaging and phase extension procedure was done without prior solvent flipping, the resulting electron density maps were inferior. The model was built using O (*13*) and refined as described (*13*).

Data set	Resolution (Å)	Complete (%)*	R_{merge}(%)†	I/σI	rms f_h/E‡
Native I	2.9	97.0 (83.0)	10.7 (29.7)	27.9 (3.2)	
Native II	2.8	96.0 (76.0)	6.6 (45.3)	24.7 (2.5)	
Mercury acetate					
1	3.4	94.4 (97.5)	13.6 (30.4)	10.8 (4.4)	3.0
2	4.0	94.4 (97.2)	17.9 (35.5)	6.8 (3.3)	2.2
3	3.4	98.5 (99.1)	13.2 (32.4)	9.9 (3.9)	2.8
4	3.2	97.7 (93.3)	7.8 (30.8)	19.1 (4.3)	1.9
PIP§					
1	3.7	91.8 (77.3)	5.7 (35.4)	22.1 (3.5)	1.1
2	3.2	98.5 (97.7)	7.3 (33.6)	22.0 (4.1)	0.8
3	3.6	95.4 (96.4)	8.1 (29.5)	20.8 (5.2)	1.0
K_2PtCl_4	4.0	98.8 (99.3)	13.0 (39.5)	10.1 (3.1)	1.5

Refinement statistics

Resolution (Å)		20.0–2.8	rms ΔB bonded NCS atoms (Å^2)#	14.4, 15.4, 19.0
Reflections in working set	$\|F\| > 0$	37148	rms Δφ all NCS residues (degrees)#	2.4, 3.2, 3.7
Reflections in test set	$\|F\| > 0$	1970	rms Δψ all NCS residues (degrees)#	2.0, 2.3, 2.4
R_{free} (%) ‖		28.8		
R_{cryst} (%) ¶		22.9	Number of nonhydrogen atoms	
rms deviations from ideal			Protein	8866
Bond lengths (Å)		0.008	Carbohydrate	388
Bond angles (degrees)		1.35	Nonglycine residues in allowed regions of Ramachandran plot as defined (*13*)	96%

*Complete = (number of independent reflections)/total theoretical number. †R_{merge} (I) = $[\Sigma|I(i) - \langle I(h)\rangle|/\Sigma I(i)]$, where I(i) is the *i*th observation of the intensity of the hkl reflection and ⟨I⟩ is the mean intensity from multiple measurements of the hkl reflection. ‡rms f_h/E (phasing power), where f_h is the heavy-atom structure factor amplitude and *E* is the residual lack of closure error. §PIP, di-m-iodobis(ethylenediamine)diplatinum nitrate. ‖R_{free} is calculated over reflections in a test set not included in atomic refinement. ¶R_{cryst} $(F) = \Sigma_h||F_{obs}(h)| - |F_{calc}(h)||/\Sigma_h|F_{obs}(h)|$, where $|F_{obs}(h)|$ and $|F_{calc}(h)|$ are the observed and calculated structure factor amplitudes for the hkl reflection. #Statistics for NCS-related residues refer to differences relative to molecule 1 for the other three molecules in the crystallographic asymmetric unit.

ZAG groove includes an unidentified nonpeptidic ligand that may be relevant for ZAG's function in lipid catabolism.

ZAG was purified from human serum and crystallized as described (*9*). The crystal structure was determined by multiple isomorphous replacement with anomalous scattering (MIRAS) aided by fourfold noncrystallographic symmetry (NCS) averaging (Table 1) (*13*). The overall structure of ZAG is similar to those of class I MHC heavy chains (Fig. 1A). The α1-α2 superdomains of ZAG, class I, and class I–related proteins form a single eight-stranded antiparallel β sheet topped by two α helices, and the α3 domain adopts a fold resembling immunoglobulin constant domains (*5, 11*). Electron density corresponding to carbohydrate is present at three of the four potential N-linked glycosylation sites in ZAG, with an unusually large number of ordered carbohydrate residues visible at Asn^{239} (Fig. 1B) (*14*). The α3 domain of human, but not mouse or rat, ZAG contains an RGD sequence (Arg^{231}, Gly^{232}, Asp^{233}) suggested to be involved in cell adhesion (*15*). However, unlike the RGD sequences in characterized adhesion molecules such as fibronectin III domains (*15*), the ZAG RGD is located in a β strand rather than a loop.

The quaternary arrangement of the ZAG α3 domain with respect to the α1-α2 platform differs from that found in β_2M-binding class I and class I–related proteins. The overall shape of ZAG is similar to an inverted "L," in which the long axis of the α3 domain is roughly perpendicular to the flat side of the α1-α2 platform, whereas the comparable angle is acute in β_2M-binding proteins (Fig. 2A). In those proteins, β_2M interacts with the α3 domain and the underside of the α1-α2 platform and is typically required for stability (*16*). The displacement of the ZAG α3 domain compared to its class I counterpart results in the inability of β_2M to optimally contact the α3 and α1-α2 domains of ZAG (*17*), contributing to ZAG's lack of affinity for β_2M. The high thermal stability of ZAG in the absence of β_2M (*9*) can be explained by a network of hydrogen bonds between α3 and α1-α2 that are not present in β_2M-binding class I proteins (Fig. 2B). In addition to the extra hydrogen bonds, the loop connecting β strand 4 to the helical region of the ZAG α1 domain platform (residues 51 to 54) and the loop connecting strands D to E in the α3 domain (residues 236 to 241) are closer together than their class I counterparts, contributing to the burial of a larger interdomain surface in ZAG (970 $Å^2$ total) than in classical class I molecules (660 $Å^2$ in HLA-A2) (*11*). There is some flexibility in the position of the ZAG α3 domain relative to α1-α2, as demonstrated by different interdomain relationships of the four ZAG molecules in the crystallographic asymmetric unit (Fig. 2A), yet ZAG is not particularly protease-sensitive at the platform-α3 hinge or any other region (*18*). Although the quaternary structure of ZAG differs significantly from the heavy chains of class I and class I–like structures, the differences are less than anticipated from the absence of the β_2M light chain. The overall similarity between ZAG and class I MHC heavy chains contrasts with the large interdomain rearrangements observed in the crystal structure of MIC-A (*10*).

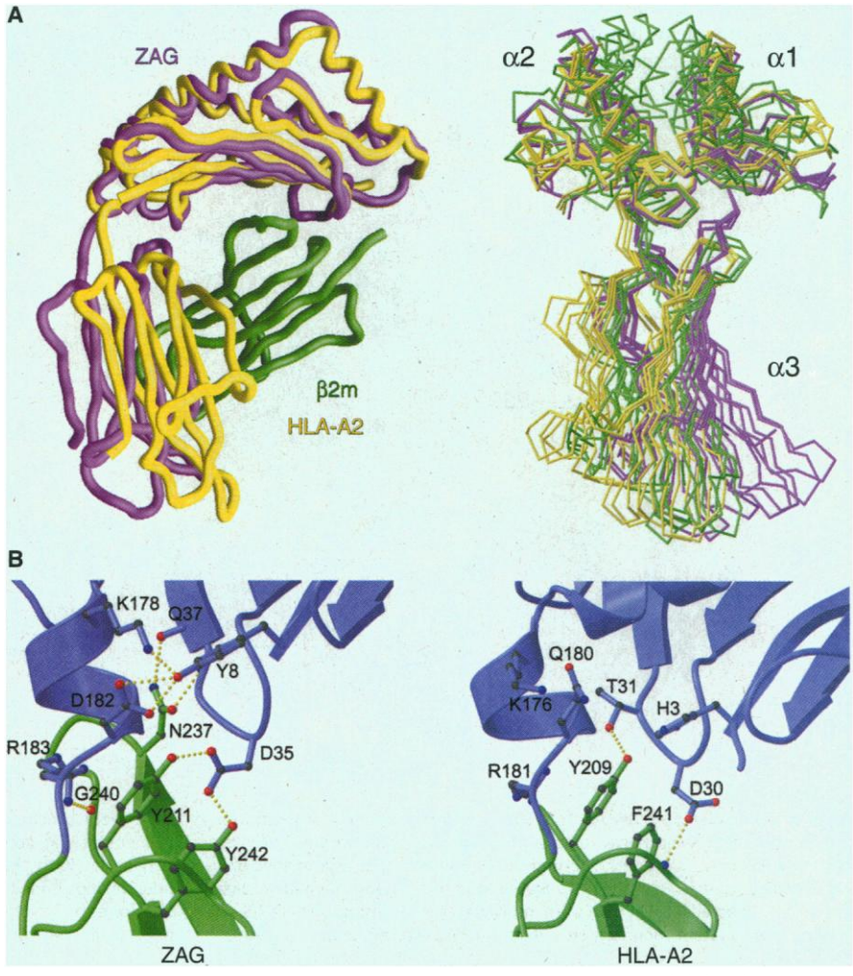

Fig. 2. Structural comparisons of ZAG, class I, and class I–related proteins. (**A**) (Left) Comparison of the structures of ZAG and HLA-A2 (*11*). (Right) Comparison of the four ZAG molecules in the crystallographic asymmetric unit (magenta) with the heavy chains of human class I MHC (yellow; PDB codes 1hhh, 1vac, 2clr) and β_2M-binding class I MHC homologs (green; FcRn, CD1, HFE) (*11*). Superpositions were based on the Cα atoms in the platform domains, using 2clr as a reference molecule. The position of the ZAG α3 domain with respect to its α1-α2 platform falls out of the range of the positions of the α3 domains of the β_2M-binding class I proteins. Differences in the platform-α3 interdomain relationships in the four ZAG molecules demonstrate that there is flexibility in the position of the ZAG α3 domain relative to α1-α2. However, the overall similarity of the four molecules, which are subjected to different crystal packing forces, rule out that ZAG's shape is an artifact of crystallization. (**B**) Close-up comparison of the interface between α1-α2 (blue) and α3 (green) in ZAG and HLA-A2 (*11*). Additional H-bonds and a larger interdomain surface area stabilize ZAG compared with class I molecules, whose heavy chains are stabilized by interactions with β_2M. Figures were made as described (*23*).

Despite the similarity between ZAG and class I molecules, structural features of the ZAG α3 domain make it unlikely to associate with the T cell coreceptor CD8. Of 15 class I heavy-chain residues identified at the CD8 binding site in the HLA-A2/CD8 cocrystal structure (*19*), only one is conserved between class I and ZAG sequences (class I Asp^{122}, ZAG Asp^{123}) (*4*). It is not possible to rule out an interaction between ZAG and T cell receptors, because the class I MHC residues that contact these receptors are not particularly conserved (*20*).

Although ZAG does not associate with peptides (*9*), the helices in both the α1 and α2 domains are almost identically positioned to their counterparts in peptide-binding class I MHC molecules (Fig. 3A) (*21*). Thus, the ZAG platform includes an open groove, by contrast to the narrowed or closed grooves observed in other class I homologs that do not bind peptides

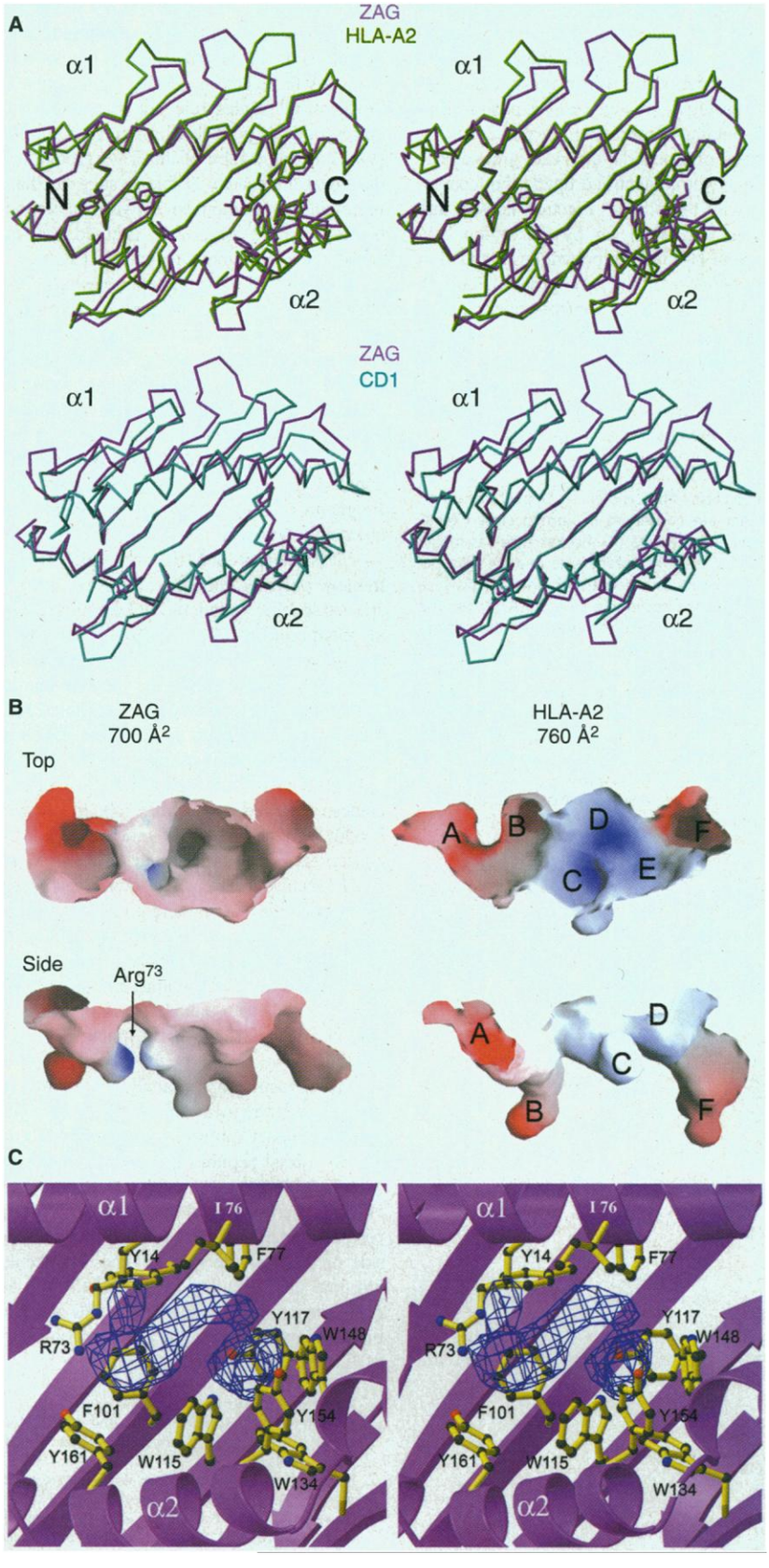

Fig. 3. Comparisons of the grooves of ZAG, class I, and class I–related proteins. (**A**) Stereoview comparisons of the α1-α2 platforms of ZAG and class I proteins that contain open antigen-binding grooves. (Top) ZAG is compared with HLA-A2, a classical class I MHC molecule. "N" and "C" indicate the orientation with respect to the NH_2- and COOH-termini of a peptide bound in the HLA-A2 groove. Side chains in common between the ZAG and HLA-A2 grooves (Table 2) are highlighted on the Cα backbones. Although many of the ZAG groove residues are chemically identical to their counterparts in HLA-A2, the conformations of the side chain, the backbone, or both, of these residues are generally different; thus, the grooves have different shapes [see (B)]. (Bottom) Comparison of ZAG and CD1. Although the ZAG and CD1 grooves both bind nonpeptidic ligands, the ZAG groove is smaller and shallower. Prolines within the α2 domain helices of ZAG (Pro^{167}) and CD1 (Pro^{169}) are highlighted. The proline in the ZAG helix is accommodated without significant distortion (*24*), as previously seen for the analogous proline within the HFE helix (Pro^{166}) (*11*). (**B**) Extruded groove pockets of ZAG and HLA-A2. Cut-away groove molecular surfaces (*11*) are shown from above (top) and the side (bottom) with electrostatic potentials (*23*), in which positive potential is blue, neutral is white, and negative potential is red. The approximate locations of pockets A through F (Table 2) are indicated on the HLA-A2 surfaces. The molecular surface of the central portion of the ZAG groove is nearly neutral except for the contribution of Arg^{73} and, like CD1 (*11*), is hydrophobic compared to the grooves of the class I molecules. Calculated groove surface areas (*11*) are indicated for ZAG and HLA-A2. For comparison, the groove surface areas for other MHC homologs are ~1440 Å² (CD1), ~235 Å² (FcRn), and ~415 Å² (HFE) (*11*). (**C**) Stereoview of electron density (from a 2.9 Å MIRAS, NCS averaged, figure-of-merit weighted electron density map contoured at 1σ) corresponding to the ZAG ligand superimposed upon a ribbon diagram of the ZAG α1-α2 platform. Residues within 4.5 Å of the density (Table 2) are highlighted in ball-and-stick representation. Figures were made as described (*23*).

[FcRn (*11*), HFE (*11*), and MIC-A (*10*)]. Despite the fact that most of the residues within the COOH-terminal portion of the ZAG α2 domain helix are chemically identical to their class I counterparts (Table 2), the ZAG groove has a different shape than a typical class I MHC peptide-binding groove (Fig. 3B). Differences in side chain conformations (Fig. 3A) and side chain substitutions create the altered shape of the ZAG groove, which can be described as containing three pockets: a large, predominantly hydrophobic central pocket and two smaller, more acidic flanking pockets (Fig. 3B). The boundary on the left of the central pocket (Fig. 3B) is created by the side chain of Arg^{73}, which points into the groove to separate the central and left pockets. Class I MHC grooves contain a smaller side chain at this position (His^{70} in HLA-A2) (*4*). Because of Arg^{73} and other side chain substitutions or conformational differences relative to class I molecules, the ZAG groove cannot accommodate even a polyalanine version of an eight- or nine-residue peptide in a class I–binding conformation (Table 2).

Instead of a peptide, the ZAG groove contains an as yet unidentified ligand that cocrystallizes with the protein. Electron density that cannot be accounted for by the amino acid sequence or N-linked carbohydrates is found in the central pocket of the ZAG groove (Figs. 1A and 3C). The density is a curved nonbranched tube, lacking the characteristic protrusions of peptides, that is situated near a cluster of hydrophobic amino acids (three tryptophans, four tyrosines, an isoleucine, and two phenylalanines) and the positively charged side chain of Arg^{73} (Table 2). Although it is not possible to unambiguously identify the compound or compounds in the ZAG groove at the current resolution of the electron density maps, previous biochemical studies rule out that the density corresponds to peptide or mixture of peptides (*9*). The composition of the ZAG groove residues near the density (Table 2) suggests that it represents one or more small hydrophobic molecules, perhaps negatively charged. Chloroform-methanol extractions and acid eluates of ZAG as well as the intact protein have been analyzed by gas chromatography, electrospray, or matrix-assisted laser desorption/ionization mass spectrometry, or a combination of these methods (*22*). The ligand has not yet been detected, but in the absence of information about the chemical nature, size, and ionic state of the ligand, these results cannot be considered conclusive. Electrospray analyses of proteolytic fragments of ZAG reveal that the ligand is not covalently bound (*22*).

Classical class I MHC molecules are extremely polymorphic, whereas ZAG exhibits species-specific variations but little or no genetic polymorphism (*4, 5*). Most of the allele-specific variations of class I MHC molecules map to residues within the peptide-binding groove that interact with peptides (Table 2) (*5*). This property of class I molecules results in allele-specific peptide-binding motifs, such that individual class I molecules show distinct preferences for binding peptides (*5*). In contrast, residues within the ZAG groove are mostly conserved, and those residues closest to the ZAG ligand are completely conserved (Table 2), even though human and rodent ZAG share only ~56% sequence identity (*4*). Taken together with ZAG's lack of polymorphism, these observations imply that human and rodent ZAG carry a single compound, or single class of compounds, related to their function in lipid catabolism.

The crystallographic analysis of ZAG reveals a structure with surprising similarity to classical class I molecules despite ZAG's inability to bind peptides or β_2M (*9*). ZAG and MHC-related proteins such as FcRn (*11*) and HFE (*11*) have adapted the same basic fold to perform widely different roles within and outside of the immune system. These molecules illustrate the versatility of the MHC fold and raise intriguing questions about the ancestral function and evolutionary relationships of MHC and MHC-related proteins.

Table 2. Comparison of residues in α1-α2 grooves of ZAG and a class I MHC molecule. Uppercase letters in any of the HLA-A2 and ZAG columns indicate residues that are conserved in human class I MHC sequences (*4*) or residues that are conserved in human, mouse, and rat ZAG (*4*). Pocket residues in the peptide-binding groove of HLA-A2 are defined as having ≥5.0 Å^2 accessible surface area to a 1.4 Å probe, but <5.0 Å^2 accessible surface area to a 5 Å probe (*11*). HLA-A2 residues marked with an asterisk were originally defined as pocket residues by M. A. Saper *et al.* (*11*) but are accessible to a 5.0 Å probe. The HLA-A2 residues designated as "NONE" (conserved) or "none" (not conserved) do not meet the criteria for being in a pocket, but are listed for comparison with ZAG. Pocket letter names (uppercase letters, conserved residues) refer to well-characterized pockets in the peptide-binding grooves of class I MHC molecules (*5, 11*). ZAG residues analogous to class I pocket residues are designated as "POCKET" (conserved) or "pocket" (not conserved) if they meet the criteria for pocket residues in HLA-A2, "BURIED" or "buried" if they have ≤5.0 Å^2 accessible surface area to a 1.4 Å probe and ≤5.0 Å^2 accessible surface area to a 5 Å probe, and "EXPOSED" or "exposed" if they have ≥5.0 Å^2 accessible surface area to a 1.4 Å probe and ≥5.0 Å^2 accessible surface area to a 5 Å probe. Surface areas were calculated (*11*) using the coordinates of HLA-A2 (excluding water molecules and bound peptide) and ZAG. Steric clashes with polyalanine peptides bound to ZAG in their class I–binding configuration were defined as described in the structural analysis of HFE (*11*).

HLA-A2	Pocket	ZAG	Pocket	Clash with peptide?	≤4.5 Å of ZAG ligand?
MET-5	A	LEU-10	BURIED	NO	NO
TYR-7	A,B	tyr-12	pocket	yes	no
phe-9	b,c	TYR-14	POCKET	NO	YES
met-45	b	ser-48	pocket	no	no
tyr-59	a	ASP-62	EXPOSED	NO	NO
glu-63	a,b	asp-66	pocket	no	no
lys-66*	a	LEU-69	EXPOSED	YES	NO
val-67	b	GLN-70	POCKET	YES	NO
his-70	b,c	ARG-73	POCKET	YES	YES
thr-73*	c	ILE-76	EXPOSED	YES	YES
his-74	none	PHE-77	POCKET	NO	YES
val-76	none	glu-79	exposed	yes	no
asp-77*	f	THR-80	POCKET	YES	NO
thr-80*	f	ASP-83	EXPOSED	YES	NO
leu-81	f	ILE-84	POCKET	NO	NO
arg-97	c,e	GLY-99	POCKET	NO	NO
tyr-99	a,b,c,d	PHE-101	POCKET	NO	YES
his-114	c,d,e	TRP-115	POCKET	NO	YES
tyr-116	c,f	TYR-117	POCKET	NO	YES
TYR-118	F	TYR-119	POCKET	NO	NO
TYR-123	F	tyr-124	pocket	no	no
ILE-124	F	ILE-125	BURIED	NO	NO
TRP-133	NONE	TRP-134	POCKET	NO	YES
thr-143	f	THR-144	POCKET	YES	NO
LYS-146	NONE	LYS-147	EXPOSED	YES	NO
trp-147	e,f	TRP-148	POCKET	NO	YES
val-152	e	TYR-154	EXPOSED	NO	YES
leu-156	d,e	ALA-158	POCKET	NO	NO
TYR-159	A,D	TYR-161	POCKET	YES	YES
trp-167	a	thr-169	pocket	yes	no
tyr-171	a	TYR-173	POCKET	YES	NO

References and Notes

1. W. Bürgi and K. Schmid, *J. Biol. Chem.* **236**, 1066 (1961); T. Tada *et al.*, *J. Histochem. Cytochem.* **39**, 1221 (1991).
2. N. J. Bundred, W. R. Miller, R. A. Walker, *Histopathology* **11**, 603 (1987); J. P. Freije, A. Fueyo, J. Uría, C. López-Otín, *FEBS Lett.* **290**, 247 (1991); L. M. Sánchez, F. Vizoso, I. Díez-Itza, C. López-Otín, *Cancer Res.* **52**, 95 (1992); I. Díez-Itza *et al.*, *Eur. J. Cancer* **9**, 1256 (1993); Y. S. López-Boado, I. Díez-Itza, J. Tolivia, C. López-Otín, *Breast Cancer Res. Treat.* **29**, 247 (1994).

3. P. T. Todorov *et al.*, *Cancer Res.* **58**, 2353 (1998); K. Hirai, H. J. Hussey, M. D. Barber, S. A. Price, M. J. Tisdale, *ibid.*, p. 2359.
4. Protein sequences: Human ZAG [T. Araki *et al.*, *Proc. Natl. Acad. Sci. U.S.A.* **85**, 679 (1988)]; mouse ZAG [H. Ueyama, H. Naitoh, I. Ohkubo, *J. Biochem.* **116**, 677 (1994)]; rat ZAG [A. Fueyo, J. A. Uría, J. P. Freije, C. López-Otín, *Gene* **145**, 245 (1994)]. Human class I MHC sequences [P. J. Bjorkman and P. Parham, *Annu. Rev. Biochem.* **59**, 253 (1990)]; MHC homolog sequences, SWISS-PROT [A. Bairoch and R. Apweiler, *Nucleic Acids Res.* **26**, 38 (1998)]. Sequence identities: ZAG and HLA-A2, 36%; ZAG and FcRn, 27%; ZAG and mouse CD1d, 23%; ZAG and HFE, 36%; ZAG and MIC-A, 29%.
5. D. R. Madden, *Annu. Rev. Immunol.* **13**, 587 (1995).
6. E. M. Beckman *et al.*, *Nature* **372**, 691 (1994); A. R. Castaño *et al.*, *Science* **269**, 223 (1995).
7. R. P. Junghans, *Immunol. Res.* **16**, 29 (1997); V. Ghetie and E. S. Ward, *Immunol. Today* **18**, 592 (1997); N. E. Simister, E. J. Israel, J. C. Ahouse, C. M. Story, *Biochem. Soc. Trans.* **25**, 481 (1997).
8. J. N. Feder *et al.*, *Nature Genet.* **13**, 399 (1996); J. N. Feder *et al.*, *Proc. Natl. Acad. Sci. U.S.A.* **95**, 1472 (1998).
9. L. M. Sánchez, C. López-Otín, P. J. Bjorkman, *Proc. Natl. Acad. Sci. U.S.A.* **94**, 4626 (1997). In thermal denaturation studies, ZAG denatures with a transition midpoint of 65°C, compared to 57°C for the peptide-filled class I molecule H-2K^d and 45°C for empty K^d [M. L. Fahnestock, I. Tamir, L. Narhi, P. J. Bjorkman, *Science* **258**, 1658 (1992)].
10. V. Groh *et al.*, *Proc. Natl. Acad. Sci. U.S.A.* **93**, 12445 (1996). The crystal structure of MIC-A reveals a major rearrangement in domain organization compared to the structures of class I molecules and ZAG. The MIC-A α1-α2 platform is displaced from its α3 domain by 113.5° compared to class I molecules. As a result, the MIC-A α1-α2 platform makes no contact with its α3 domain [P. Li, S. T. Willie, S. Bauer, D. L. Morris, T. Spies, R. K. Strong, personal communication].
11. Protein structures: HLA-A2 [Protein Data Bank (PDB) code 2CLR] [E. J. Collins, D. N. Garboczi, D. C. Wiley, *Nature* **371**, 626 (1994)]; Mouse CD1 (PDB code 1CD1) [Z.-H. Zeng *et al.*, *Science* **277**, 339 (1997)]; Rat FcRn (PDB code 3FRU) [W. P. Burmeister, L. N. Gastinel, N. E. Simister, M. L. Blum, P. J. Bjorkman, *Nature* **372**, 336 (1994)]; Human HFE (PDB code 1A6Z) [J. A. Lebrón *et al.*, *Cell* **93**, 111 (1998)]. Molecular surface areas buried by interaction were calculated with X-PLOR [A. T. Brünger, *X-PLOR. Version 3.1: A System for X-ray and NMR* (Yale Univ. Press, New Haven, CT, 1992)] with a 1.4 Å radius. Identification of pocket residues and calculation of groove surface areas were done based upon earlier analyses of human and mouse class I structures [M. A. Saper, P. J. Bjorkman, D. C. Wiley, *J. Mol. Biol.* **219**, 277 (1991); M. Matsumura, D. H. Fremont, P. A. Peterson, I. A. Wilson, *Science* **257**, 927 (1992)] as described in the CD1 (Z.-H. Zeng *et al.*) and HFE (J. A. Lebrón *et al.*) structure papers. Cut away molecular surfaces of grooves (Fig. 3B) were generated as described in the CD1 structure paper.
12. S. Shibata and K. Miura, *Nephron* **31**, 170 (1982).
13. Structure determination and refinement: HKL [Z. Otwinowski and W. Minor, *Methods Enzymol.* **276**, 307 (1997)]. SHARP [E. De La Fortelle and G. Bricogne, *ibid.*, p. 472]. Solomon [J. P. Abrahams and A. G. W. Leslie, *Acta Crystallogr. D* **52**, 30 (1996)]. CCP4 programs [CCP4: Collaborative Computational Project No. 4, Daresbury, UK, *Acta Crystallogr. D* **50**, 760 (1994)]. O [T. A. Jones and M. Kjeldgaard, *Methods Enzymol.* **277**, 173 (1997)]. R_{free} [A. T. Brünger, *Nature* **355**, 472 (1992)]. The Native II data set (Table 1) was used for refinement. After rigid-body refinement of eight domains in the asymmetric unit (α1-α2 and α3 for each of four ZAG molecules) using CNS [A. T. Brünger *et al.*, *Acta Crystallogr. D* **54**, 905 (1998)], the four molecules were subjected to restrained NCS torsion-angle refinement using the maximum likelihood target function. Tight NCS restraints (300 kcal/mol·Å^2) were applied to all regions except for flexible loops and residues involved in lattice contacts. Intermediate rounds of model building and refinement included the calculation of SIGMAA-weighted [R. J. Read, *Acta Crystallogr. A* **42**, 140 (1986)] simulated annealing omit maps [A. Hodel, S.-H. Kim, A. T. Brünger, *Acta Crystallogr. A* **48**, 851 (1992)]. Final rounds of rebuilding and refinement included tightly restrained individual atomic temperature factor refinement (temperature factor rms deviation for bonded main chain and side chain atoms is 5.7 and 8.8 Å^2, respectively). The model consists of residues 5 through 277 (average *B*: 48 Å^2) with nine carbohydrate residues (average *B*: 61 Å^2) for molecule 1, residues 5 through 278 (average *B*: 56 Å^2) with 11 carbohydrate residues (average *B*: 80 Å^2) for molecule 2, residues 6 through 278 (average *B*: 57 Å^2) with four carbohydrate residues (average *B*: 107 Å^2) for molecule 3, and residues 6 through 249 and 258 through 276 (average *B*: 62 Å^2) with five carbohydrate residues (average *B*: 90 Å^2) for molecule 4 (Wilson B = 64 Å^2). Excluding regions that deviate from the NCS, the domains in the NCS-related ZAG monomers are very similar (<0.04 Å rms deviation for Cα atoms). Ramachandran plot statistics (Table 1) are as defined by G. J. Kleywegt and T. A. Jones [*Structure* **4**, 1395 (1996)].
14. Extensive carbohydrate density is found at Asn^{239} (nine ordered carbohydrate residues in molecule 2) and to a much lesser extent at Asn^{89} and Asn^{108} in all four ZAG molecules (Fig. 1) (*13*). Crystal structures of glycoproteins rarely show more than three ordered carbohydrate residues at each glycosylation site [D. E. Vaughn and P. J. Bjorkman, *Structure* **6**, 63 (1998)]. The Asn in the fourth potential N-linked glycosylation site (Asn^{92}) does not show density corresponding to carbohydrate. The bond between Asn^{92} and Gly^{93} can be cleaved by hydroxylamine, confirming that Asn^{92} is not glycosylated (*18*).
15. M. Takagaki *et al.*, *Biochem. Biophys. Res. Commun.* **201**, 1339 (1994); O. Ogikubo *et al.*, *ibid.* **252**, 257 (1998); M. Pfaff, in *Integrin-Ligand Interaction*, J. A. Eble and K. Kühn, Eds. (Chapman & Hall, New York, 1997), pp. 101–121.
16. V. A. Tysoe-Calnon, J. E. Grundy, S. J. Perkins, *Biochem. J.* **277**, 359 (1991); D. Lancet, P. Parham, J. L. Strominger, *Proc. Natl. Acad. Sci. U.S.A.* **76**, 3844 (1979); A. Bauer *et al.*, *Eur. J. Immunol.* **27**, 1366 (1997).
17. Structural features that prevent ZAG from binding β_2M include the following residues, which clash with β_2M when it is positioned on the ZAG structure either by interacting with α3 or with α1-α2: Ile^{13}, Thr^{15}, Leu^{30}, Arg^{40}, Gln^{98}, Tyr^{118}, Lys^{122}, Val^{234}, His^{236}, Trp^{245}.
18. L. M. Sánchez and P. J. Bjorkman, unpublished results.
19. G. F. Gao *et al.*, *Nature* **387**, 630 (1997).
20. D. N. Garboczi *et al.*, *ibid.* **384**, 134 (1996); K. C. Garcia *et al.*, *Science* **274**, 209 (1996); Y. H. Ding *et al.*, *Immunity* **8**, 403 (1998); K. C. Garcia *et al.*, *Science* **279**, 1166 (1998).
21. Superpositions based on Cα atoms in the platform β strands reveal that the ZAG platform is more similar to classical class I MHC molecules than to any of the class I homologs [rms deviations for superpositions of platforms: ZAG and HLA-A2, 1.3 Å (147 Cα atoms); ZAG and CD1, 1.1 Å (86 Cα atoms); ZAG and FcRn 1.0 Å (88 Cα atoms); ZAG and HFE 1.0 Å (115 Cα atoms)].
22. L. M. Sánchez, A. J. Chirino, P. J. Bjorkman, G. Hathaway, P. G. Green, K. Faull, unpublished results.
23. Figures 1, 2A (right), 2B, 3A, and 3C were made using MOLSCRIPT [P. J. Kraulis, *J. Appl. Crystallogr.* **24**, 946 (1991)] and RASTER-3D [E. A. Merritt and M. E. P. Murphy, *Acta Crystallogr. D.* **50**, 869 (1994)]. Electrostatic calculations were done and Figs. 2A (left) and 3B were made using GRASP [A. Nicholls, R. Bharadwaj, B. Honig, *Biophys. J.* **64**, A166 (1993)].
24. ZAG, CD1, HFE, and FcRn contain prolines within their α2 domain helices at a position corresponding to Val^{165} in classical class I MHC molecules (*4*). The FcRn and CD1 helices are kinked at a position near their proline residues, whereas the ZAG and HFE helices are similar to the α2 domain helices of class I molecules (*11*). Substitution of Val^{165} for proline in the mouse class I molecule H-2D^d did not interfere with binding and presentation of peptides to T cells, suggesting that no major structural rearrangements occurred [D. Plaksin, K. Polakova, M. G. Mage, D. H. Margulies, *J. Immunol.* **159**, 4408 (1997)].

25. We thank G. Hathaway, P. G. Green, and K. Faull for mass spectrometric analyses. ZAG coordinates have been deposited in the PDB (code 1zag). L.M.S. was supported by a grant from the U.S. Department of Defense Breast Cancer Research Program.

21 December 1998; accepted 18 February 1999

Acoel Flatworms: Earliest Extant Bilaterian Metazoans, Not Members of Platyhelminthes

Iñaki Ruiz-Trillo,[1] Marta Riutort,[1] D. Timothy J. Littlewood,[2] Elisabeth A. Herniou,[2] Jaume Baguñà[1]*

Because of their simple organization the Acoela have been considered to be either primitive bilaterians or descendants of coelomates through secondary loss of derived features. Sequence data of 18S ribosomal DNA genes from non–fast evolving species of acoels and other metazoans reveal that this group does not belong to the Platyhelminthes but represents the extant members of the earliest divergent Bilateria, an interpretation that is supported by recent studies on the embryonic cleavage pattern and nervous system of acoels. This study has implications for understanding the evolution of major body plans, and for perceptions of the Cambrian evolutionary explosion.

"Since the first Metazoa were almost certainly radial animals, the Bilateria must have sprung from a radial ancestor, and there must have been an alteration from radial to bilateral symmetry. This change constitutes a most difficult gap for phylogeneticists to bridge, and various highly speculative conjectures have been made" (*1*, p. 5). So began Libbie Hyman's discussion on the origin of bilaterian Metazoa, and despite a century of morphological studies and a decade of intensive molecular work, the nature of the simplest bilaterian animal remains elusive (*1, 2*). Paleontological and molecular data indicate that most bilaterian phyla appeared and diversified during the Cambrian explosion (*3, 4*). Three main clades emerged—